Comparative Assessment of Isolated Propeller Noise Test Rigs

Beck, Augusto B. ; Teodoro, Emanoela F. ; Bonomo, Lucas A.; Cordioli, Júlio A.; Fonseca, João Victor N. ; Simões, Leandro G. C. ; Tourinho, André M. C. ; Casalino, D.; Ragni, D.

Important note
To cite this publication, please use the final published version (if applicable).
Please check the document version above.

Check for updates

Comparative Assessment of Isolated Propeller Noise Test Rigs

Augusto B. Beck*, Emanoela F. Teodoro [†], Lucas A. Bonomo[‡] and Julio A. Cordioli[§]
Federal University of Santa Catarina, Florianópolis - SC, 88040-900, Brazil

João Victor N. Fonseca[¶], Leandro G. C. Simões[‖] and André M. C. Tourinho[**]
EMBRAER S.A., São José dos Campos - SP, 12227-901, Brazil

Damiano Casalino[††] and Daniele Ragni[‡‡]
Delft University of Technology, Kluyverweg 1, 2629 HS Delft, The Netherlands

Francesco Avallone[§§]
Politecnico di Torino, 10129, Torino, Italy

Commercial aircraft electrification and novel urban air mobility vehicles under development have brought renewed interest in propeller noise to the research community. The complex noise generation mechanisms and broad range of possible configurations lead to the development of a large number of propeller noise test rigs. However, the effects of test rig configuration, installation, and instrumentation on the experimental results are still unclear. In this work, the comparison of the results obtained by two different institutes, the Federal University of Santa Catarina (Brazil) and TU Delft (The Netherlands), is presented.A pair of identical propellers, used for acoustic benchmark studies, were tested under the same conditions to compare the effects of the test rigs on the noise results. A good agreement is observed for thrust and torque. Some divergences on the acoustic data were observed. However, good agreement was noted at the first harmonic and overall sound pressure level, with a maximum difference of 1.8 and 2.8 dB, respectively.

I. Introduction

THE aeronautic sector is currently undergoing a revolution, with environmental sustainability driving the aircraft industry towards the electrification of traditional aircraft [1]. Parallel to this disruption in the traditional aircraft propulsion system, urban life in the 21st century requires solutions for human and goods and services transportation. Efforts are underway to develop flying vehicles for urban air mobility, predominantly in the form of eVTOL (electric Vertical Take-off and Landing) vehicles [2]. Additionally, small unmanned aerial vehicles have been widely deployed to perform a variety of tasks, from delivering small packages to monitoring security [3].

The advent of electric motors with easily variable RPM has led to an increase in the use of fixed pitch propellers, which still maintain good efficiency at different advance ratios [4]. Taking into account the large number of these vehicles expected to be deployed and their operational proximity to humans, noise pollution is a major concern, with the propeller playing a leading role. Propeller noise is generated from the fluid flow around the blades and has a spectrum dominated by two fundamental components, namely tonal noise and broadband noise [5]. The propeller tonal noise arises from deterministic aeroacoustic sources generated from blade loading and thickness contributions, which are bound by the fundamental Blade Passing Frequency (BPF) and its harmonics [6]. Conversely, broadband noise is a nonperiodic contribution, mainly generated by trailing-edge noise scattering and stochastic phenomena related to complex nondeterministic mechanisms, including turbulence ingestion and blade-vortex interactions [7]. Although the

---

*MSc Student, Department of Mechanical Engineering, augusto.beck@lva.ufsc.br
[†]Undergraduate Student, Department of Mechanical Engineering, emanoela.flores@lva.ufsc.br
[‡]PhD Student, Department of Mechanical Engineering, lucas.bonomo@lva.ufsc.br, AIAA Student Member.
[§]Associate Professor, Department of Mechanical Engineering, julio.cordioli@ufsc.br, AIAA Member.
[¶]Product Development Engineer, Noise and Vibration, joao.fonseca@embraer.com.br.
[‖]Product Development Engineer, Noise and Vibration, leandro.simoes@embraer.com.br.
[**]Product Development Engineer, Noise and Vibration, andre.tourinho@embraer.com.br.
[††]Professor, Faculty of Aerospace Engineering, Delft University of Technology, the Netherlands.
[‡‡]Associate Professor, Faculty of Aerospace Engineering, Delft University of Technology the Netherlands.
[§§]Full Professor, Dimes Department, francesco.avallone@polito.it, AIAA Member.

noise-generating mechanisms are well-known, the lower Reynolds numbers at which small propellers operate create new challenges in understanding and modeling the phenomena due to boundary layer transitions [8, 9].

Motivated by this new demand, a large number of propeller noise test rigs have been developed worldwide in recent years (for instance, see Refs. [10–16]). These systems are typically built into either aeroacoustic wind tunnels, for in-flight test conditions, or (semi-)anechoic chambers that allow only for hover conditions. Despite the abundance of recent publications, there is a scarcity of cross-comparisons among experimental facilities, which creates a knowledge gap regarding the impact of different setups on measured propeller noise

This collaborative study proposes a back-to-back comparison of the isolated propeller noise test rigs at the Federal University of Santa Catarina (UFSC) in Brazil and TU Delft in the Netherlands. The test conditions are limited to hover, as this regime is particularly challenging due to the propeller's sensitivity to changes in inflow.

This work presents comparisons for both loading and acoustic measurements. Loading is evaluated in the form of thrust and torque. The acoustic analysis considers sound spectra and their directivities, including both tonal and broadband noise, using separation algorithms [17], as well as the overall sound pressure level (OASPL).

This paper is organized as follows: Section II describes the experimental facilities. Section III details the test matrix considered for the study. Section IV outlines the methods used for signal processing. Section V presents the results, and Section VI offers the main conclusions.

II. Experimental Facilities

A. UFSC

The UFSC Isolated Propeller Test Rig is installed in the semi-anechoic chamber at the Laboratory of Vibration and Acoustics (LVA/UFSC). This chamber features acoustically treated walls and ceiling, with an exposed concrete floor. The interior dimensions, measured from the wedge tips of the acoustic foam, are 5.2 m by 5.2 m, and the height from the wedge tips of the acoustic foam to the concrete floor is 3.5 m. The configuration provides a cut-off frequency of 100 Hz.

The propeller rig structure primarily consists of an aluminum frame mounted on a steel column bolted to the ground, as depicted in Fig. 1a. A brushless DC motor, specifically the U3 KV700 model from T-Motor, is utilized to drive motion to the propellers, in conjunction with an Electronic Speed Controller (ESC), the ALPHA 40A, also from T-Motor. Rotational speed and angular position monitoring are facilitated by a digital laser indexed encoder, the EM1 from US Digital, with 50 cycles per revolution (CPR).

The rotational speed of the propeller is controlled via an in-house closed-loop PID controller, implemented in Python3, utilizing a PXIe-6368 Multi-function DAQ as a hardware interface. The controller operates with an average update rate of 30 Hz. Load measurements are conducted using a six-axis load cell from ATI Industrial Automation, the Mini-40 model. The load cell is factory calibrated to measure a full-scale axial force (thrust) of 60 N and a full-scale torque of 1 N m on each axis.

Structural vibration is monitored using a triaxial accelerometer from PCB Piezoelectronics, specifically the type 356A45, positioned behind the motor axis. Additionally, the test rig is equipped with two integrated-circuit temperature sensors from Texas Instruments, the LM35DZ model, to monitor temperatures at the motor base and the load cell. The instrumentation setup of the test rig is illustrated in Fig. 1b.

A flexible fixture is applied between the motor aluminum profile and the structure, which is then covered with viscoelastic material and acoustic foam to reduce mechanical vibrations. Additionally, to minimize drag-induced noise, the structure is enveloped with an aerodynamic profile, as depicted in Fig. 1a.

The vertical distance between the propeller hub and the floor is 1.2 m. An array of microphones, oriented towards the ground, is positioned in line at a distance of 1.6 m from the steel column, parallel and 2 m away from the propeller axis. The array is arranged to cover a range from $-45°$ to $45°$, with $0°$ representing the rotor disk plane and positive angles measured above the rotation plane. Comprising nine GRAS 46AE 1/2" free-field microphones, the array includes positions at angular offsets of $-27.5°$, $0°$, and $27.5°$, numbered 3, 5, and 7, respectively. Results are compared with those obtained from Delft microphones positioned at $-30°$, $0°$, and $30°$. The microphones are oriented towards the ground at a distance of 12 mm, as shown in Fig. 2. Inverting the microphone positioning helps mitigate the effects of ground reflection by subtracting 6 dB from the measured sound pressure level [18], provided the maximum frequency of interest corresponds to a wavelength $\lambda >> 12$ mm. The minimum ratio of the distance between microphones and the hub r to the propeller diameter d was $r/d \approx 6.5$, ensuring all microphones were positioned in the acoustic far field [12].

All signals are simultaneously acquired using custom software implemented in Python3, utilizing the `nidaqmx` library. The signals are acquired with PXIe-4499 modules by National Instruments, with a sampling frequency of
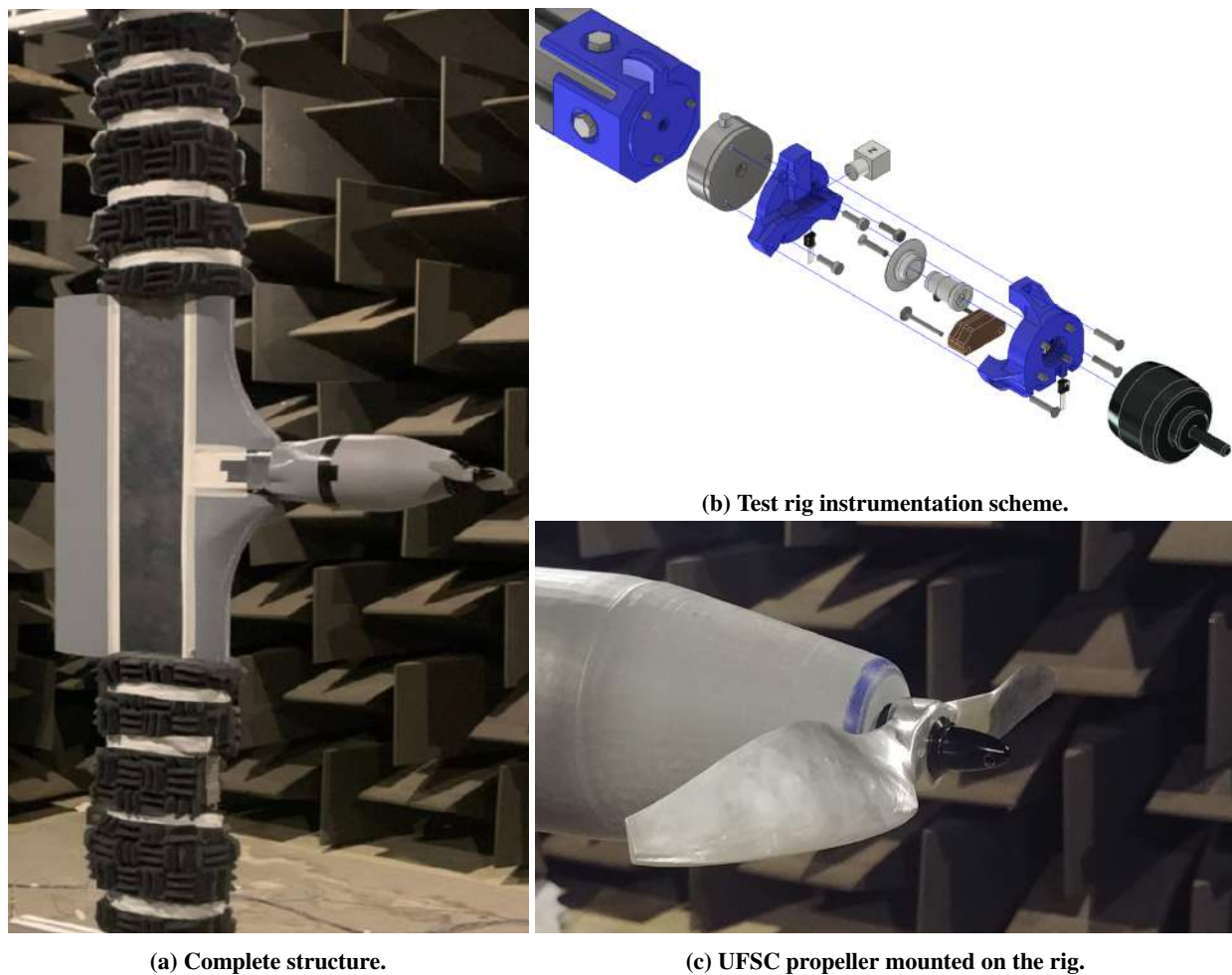
2

(a) Complete structure.

(b) Test rig instrumentation scheme.

(c) UFSC propeller mounted on the rig.

Fig. 1   UFSC propeller test rig.

51.2 kHz during 30 s runs for each test condition. However, the measurement window considered for each case will vary, as discussed in Section IV.

B. TU Delft

The propeller noise test rig at TU Delft is installed in the semi-anechoic aeroacoustic wind tunnel of Delft University of Technology (TU Delft A-Tunnel). The maximum flow speed that the A-Tunnel can provide is 35 m s^{-1}, but for the current study, only no-flow cases will be considered. The height of the semi-anechoic test chamber is 3.2 m, and the other two dimensions are 6.4 m and 4.4 m. The cut-off frequency of the chamber is approximately 200 Hz. The test rig installed in the A-Tunnel can be seen in Fig. 3a.

Power is driven to the propeller by an electrical brushless motor Leopard Hobby 3536-5T 1520 KV. US Digital EM1 optical encoder are used to measure the shaft rotational speed. Thrust is measured by means of a load cell Futek LSB200 excited with 5VDC for the thrust measurement, and characterized by a maximum capacity of 22.2 N, while torque is measured with a Transducer Techniques RTS-25 torque sensor excited with 10 VDC, characterized by a maximum capacity of 0.18 N m. The thrust and torque signals are acquired by a National Instrument acquisition board with a sampling frequency of 5 kHz and an acquisition time of 15 s.

Noise measurements are performed through 7 G.R.A.S. 46BE 1/4 inch free-field microphones mounted on a circular microphone array, sketched in Fig. 3b, with a arc radius of 1.2 m. Each microphone is positioned 10° apart, ranging from −30° to 30°, with microphone 4 located at the propeller plane. The data acquisition system consists of two National Instrument PXIe-4499 modules. A sampling frequency of 102.4 kHz and a recording time of 30 s are used for each

3

Fig. 2 UFSC microphone array.

(a) Picture of the TU Delft facility.

(b) Microphone array for the TU Delft facility.

Fig. 3 Delft propeller test rig.

measurement.

III. Test Matrix

The propeller designed by Casalino et al. [11] as an acoustic benchmark is utilized in this work. The geometry is derived from a two-bladed APC-9x6 model, with each single blade profile reshaped using a NACA4412 airfoil and resized so that $D = 300$ mm is the rotor diameter (tip radius $R_T = 150$ mm). An elliptical root section is merged with the profiled section starting from a radius of 10 mm($r/R_T = 6$ %). The hub radius is 12.5 mm. A picture of the propeller manufactured for the UFSC team is shown in Fig. 1c. Both propellers were made of aluminum alloys and manufactured

4

using CNC machining, with a surface finish between 0.4 to 0.8 μm.

Since only the hover condition is considered, the only parameter available for parametric analysis is the propeller rotational speed. For brevity, only three rotational speeds will be considered: 4000, 5000, and 6000 RPM, corresponding to Blade Passing Frequencies (BPFs) of 133.3, 166.7, and 200 Hz, respectively. Additionally, tests will be conducted without the propeller to evaluate the motor self-noise under no-load conditions.

IV. Signal Processing

As mentioned, measurements at UFSC were conducted in a sealed semi-anechoic chamber, with each measurement lasting 30 s. In this setup, the confined flow starts to recirculate after a certain period, causing disturbances in the data [19]. To ensure that the noise spectra only comprise data recorded before recirculation, spectrograms of microphone 9 (45°) alongside thrust data were analyzed for a rotational speed of 5500 RPM, as shown in Fig. 4. In the figure, the light blue represents thrust filtered by a Butterworth low-pass filter at 1.75×BPF, while the dark line corresponds to thrust filtered at 20 Hz for visualization. Recirculation effects are evident as fluctuations in thrust and an increase in the magnitude of higher-order harmonics. For the shown case, these effects occur approximately 16 s into the recording. The vertical green lines indicate the selected window, taken before recirculation occurs and after rotational speed stabilization. Additionally, a sudden shift in broadband noise and thrust is observed approximately 7 s after data recording starts, likely due to a flow transition on the propeller. This may be attributed to the laminar separation bubble that forms on this airfoil when operating at low Reynolds number [20], collapsing above a certain rotational speed, estimated to be between 5000 and 5500 RPM on the LVA-UFSC test rig.
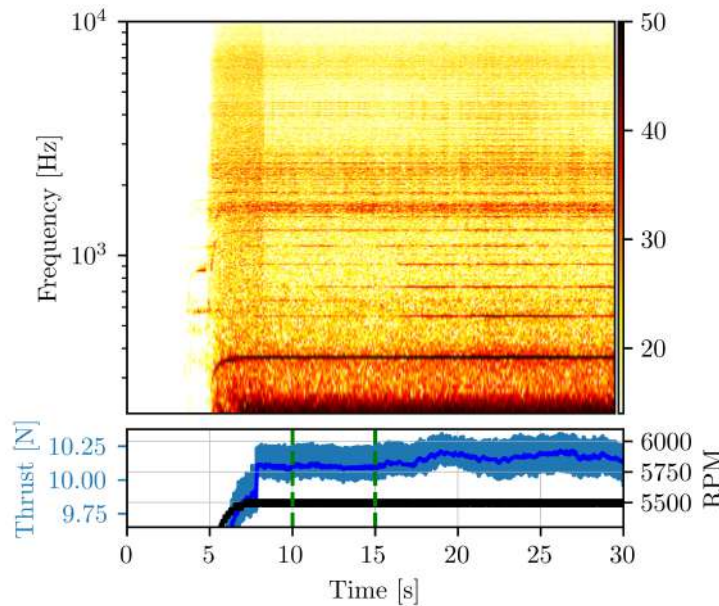

Fig. 4 Spectrogram, thrust and torque, used for selecting a section of the signal without recirculation effects.

verage thrust and torque were obtained by averaging over the selected window. A fourth-order high-pass filter with a 40 Hz cutoff frequency was applied to the microphone data. The spectra were calculated using Welch's method, with blocks of 25600 samples (dF = 2 Hz), a Hanning window, and 90 % overlap.

The tonal components were directly obtained from the spectra peaks, while broadband noise was calculated using Sree's method [21]. This method involves sectioning the full signal into blocks of approximately the same length, corresponding to one rotation based on the average RPM. Subsequently, the cross-correlation between two subsequent blocks is calculated, and the dominant phase shift is determined. The blocks are then aligned based on the phase shift and subtracted from each other, resulting in a block composed only of the random components, as depicted in the left frame of Fig. 5. A random time signal is constructed by adding the calculated blocks together. The broadband spectra is recalculated using Welch's method with the same parameters. The original and broadband spectra are compared in the right frame of Fig. 5.
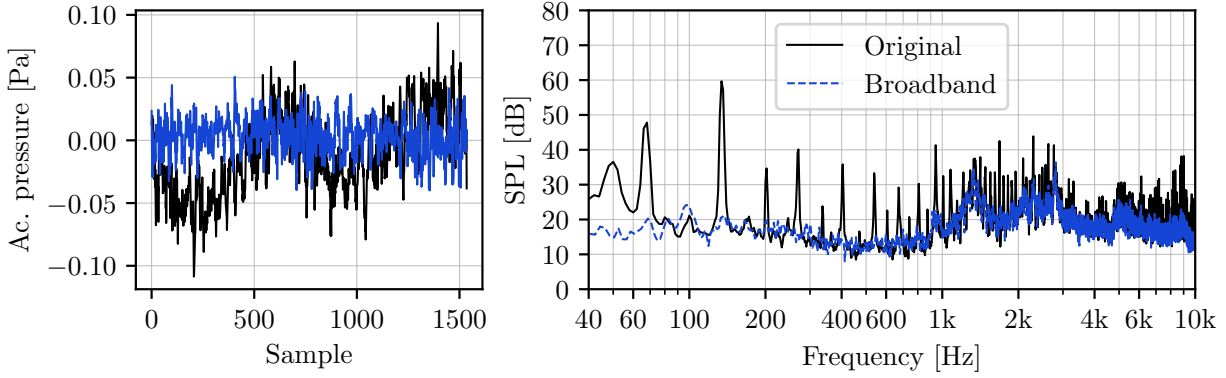
Fig. 5   Original and processed pressure time signal and spectrum, using the Sree method [21].

The overall sound pressure level (OASPL) and the broadband sound pressure level were calculated using the root mean square (RMS) value of the time signals, as follows

$$p_{\text{RMS}} = \sqrt{\frac{\sum_0^n p_i^2}{n}}, \tag{1}$$

where p_i represents the pressure time samples of the original signal *or* the signal obtained from Sree's method and n is the number of samples. The sound pressure level is then calculated by

$$\text{SPL} = 20 \log \frac{p_{RMS}}{p_0} \tag{2}$$

where $p_0 = 20\,\mu\text{Pa}$ is the reference sound pressure.

V. Results and Discussion

A. Propeller loading
We first compare the thrust and torque data from both rigs, as shown in Fig. 6, over a rotational speed range of 3000 to 6000 RPM. Overall, a good agreement is observed, with a maximum difference of 8.9 % for torque at 5000 RPM and 7.6 % for thrust at 6000 RPM. These differences may stem from various sources: Firstly, the motor fairing used on the LVA setup is significantly larger, potentially increasing the apparent thrust and torque by affecting the air being pushed against the surfaces. Additionally, Delft employs a wind tunnel to prevent recirculation, and the flow dynamics could have a slight effect on the loading.

B. Motor noise
To estimate the contributions of inherent motor noise, the unloaded motor noise is analyzed. This is particularly important for this study, as different motors are used by the two institutions. Results for 6000 RPM are shown in Fig. 7. It is worth mentioning that the unloaded and loaded motor noise will differ; therefore, this comparison is more valid from a qualitative standpoint.

The results suggest that differences in motor noise contributions between the two facilities are expected. It's important to highlight that TU Delft uses microphones with a higher noise floor, which may contribute to the measured low-frequency broadband noise being primarily microphone noise. Additionally, the motor used by TU Delft generates high-frequency broadband noise along with some medium and low-frequency tones. In contrast, the LVA-UFSC rig's motor noise spectrum is concentrated mostly in the mid-frequency bands, between 500 and 3000 Hz. The reduced high-frequency noise in the LVA-UFSC rig is likely due to the use of high-quality components such as a low-noise motor and sine wave controller, as well as the implementation of a flexible fixture and acoustic treatment of the structure. These elements help dampen the vibrations transmitted from the motor to the structure's large surface area, thereby reducing the sound produced by any residual vibrations.
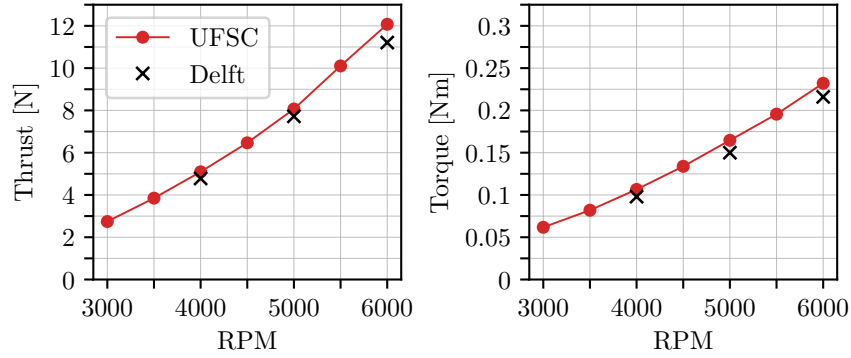
6

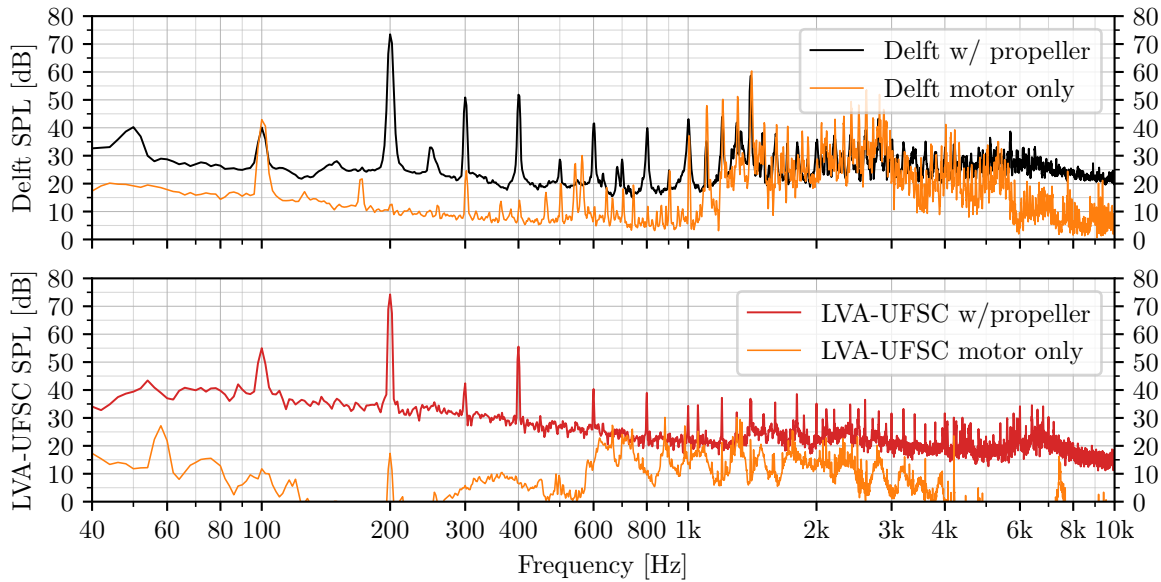**Fig. 6   Measured thrust and torque.**

Fig. 7   Propeller and motor noise spectra for 6000 RPM on both rigs.

C. Propeller noise spectra

Fig. 8 shows the spectra for 4000 RPM at both rigs, corresponding to a BPF of 133.3 Hz. The top frame compares the noise spectra for LVA's mic. 3 (−27.5°) and Delft's mic. 1 (−30°). The middle frame compares LVA's mic. 5 and Delft's mic. 4, both on the propeller plane. The third frame compares LVA's mic. 7 (27.5°) and Delft's mic. 7 (30°). The spectra levels from LVA were corrected to correspond to a distance equal to the array radius used at the Delft facility

A good agreement is observed for the first harmonic across all three polar angles, with a maximum difference of 1.8 dB. However, higher differences are observed for the second and third harmonics. Additionally, the shaft frequency odd harmonics (66.6, 200, 333.6 Hz, etc.) are present on both rigs. Notably, the second and third BPF harmonics are slightly higher in the TU Delft results, which may suggest a certain degree of flow recirculation. Similar trends have been observed in simulations of propellers under pristine and enclosed flow conditions [9].

Significant differences are observed in broadband noise between the two rigs. Below 1000 Hz, the LVA-UFSC rig displays higher noise levels, primarily originating from the wake flowing around the structure rather than from the propeller itself. In contrast, the broadband noise measured at TU Delft appears to be more accurate, despite being closer to the microphone noise floor (as seen in Fig. 7). However, the higher-frequency noise from the TU Delft facility appears to be more contaminated by motor noise compared to the LVA-UFSC measurement. Despite these differences, the spectra exhibit similarities.
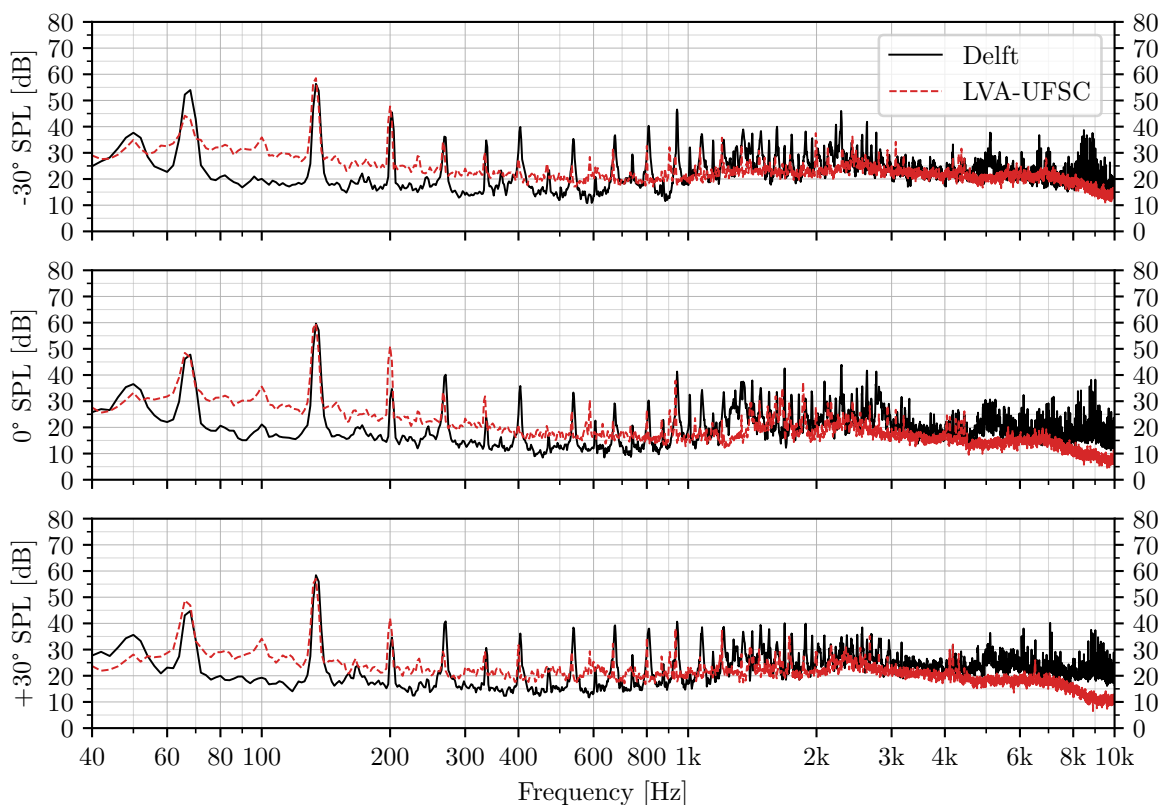
7

Fig. 8   4000 RPM spectra for -30°, 0° and 30° polar angles.

Fig. 9 displays the spectra for 5000 RPM in the first three frames and 6000 RPM in the last three frames. Once again, good agreement is observed at the first harmonic of the Blade Passing Frequency (BPF) between the two facilities. However, in contrast to the previous case, a better agreement is observed at the second harmonic of the BPF, especially at 6000 RPM.

At the rotational speed of 4000 RPM, the broadband noise differences between the rigs are similar to those observed at 5000 RPM. The measured broadband level at the LVA-UFSC rig is higher below 1000 Hz and lower above that frequency.

At a rotational speed of 5000 RPM, different patterns are observed. The low-frequency spectra difference between the two rigs is greater, while above 1200 Hz, the results are close. However, only at this rotational speed, the levels measured above 1200 Hz at TU Delft are lower than those measured at LVA-UFSC. As discussed previously and shown in Fig. 4, the flow regime observed at the UFSC test rig changes at a rotational speed around 5400 RPM, resulting in a significant change in the noise spectra, with the overall broadband noise decreasing significantly. It's worth noting that on the same rig, measuring in the pusher configuration, this transition occurred at about 4500 RPM. It is possible that on the Delft rig, this transition occurs below 5000 RPM, possibly due to differences in surrounding structures and slight propeller variations, leading to measurements being taken under different propeller flow states. It was observed that this phenomenon mainly affects broadband noise, hence the similar tonal signature.

D. Broadband noise

Fig. 10 illustrates the one-third octave band levels of the broadband spectra measured at the propeller plane for the three rotational speeds at each test rig, extracted using Sree's Method [21]. Consistently, the broadband noise at the LVA-UFSC test rig is higher (around 5 dB) at frequency bands below 1000 Hz for all RPMs. This difference is believed to stem from the interaction of the propeller wake with the larger supporting structure at LVA-UFSC compared to the Delft test rig. Conversely, above 1000 Hz, the presence of motor noise at TU Delft seems to contaminate the spectra, resulting in higher values than the LVA-UFSC results. Notably, minimal differences are observed between the
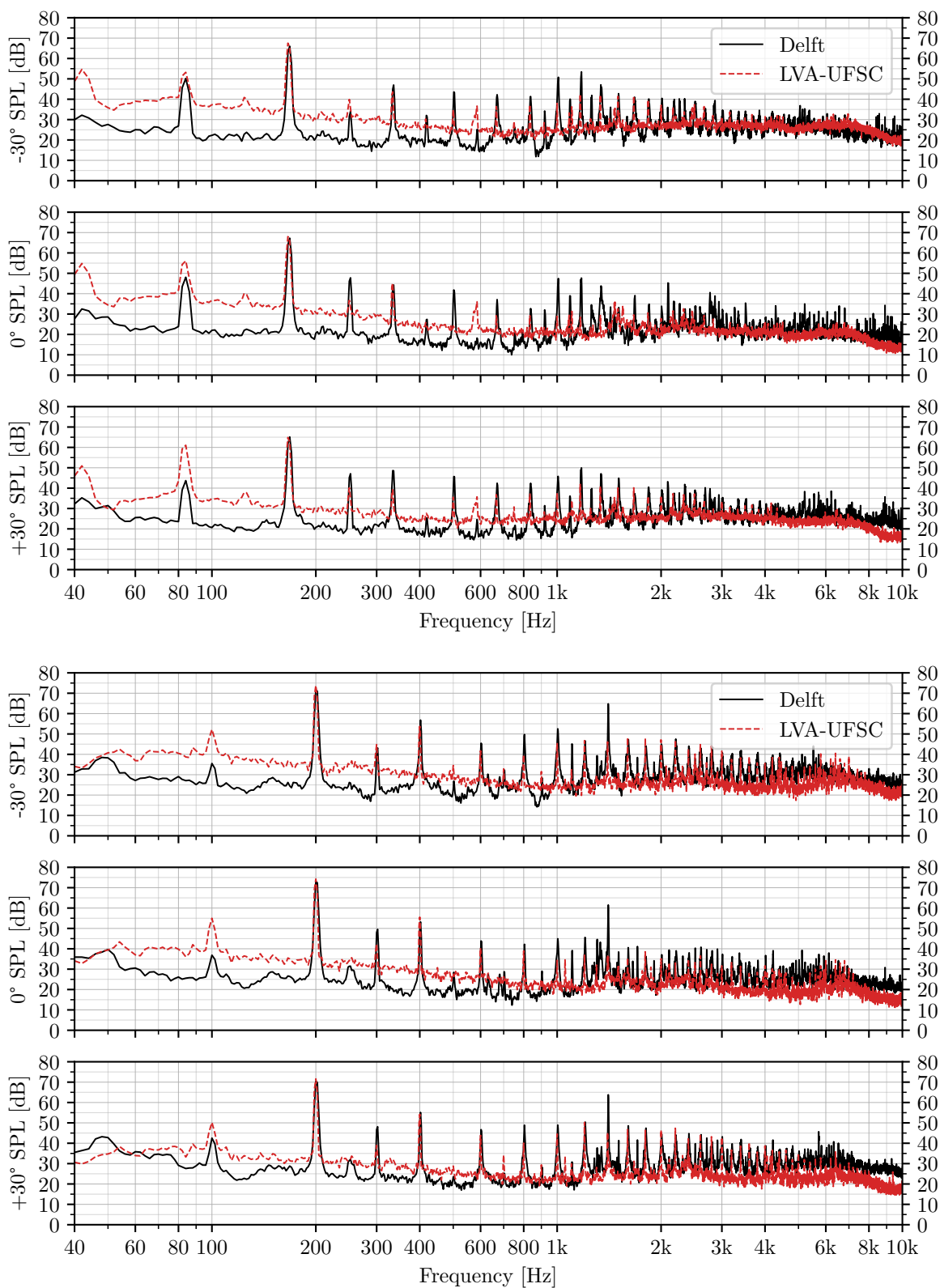
8

Fig. 9 5000 RPM **and** 6000 RPM **spectra for -**30°**,** 0° **and** 30° **polar angles.**

broadband spectra measured at Delft for 4000 RPM and 5000 RPM, as well as between 5000 RPM and 6000 RPM at UFSC. These discrepancies are attributed to the transition of the flow regime in the propeller, occurring at different RPMs at each test rig.
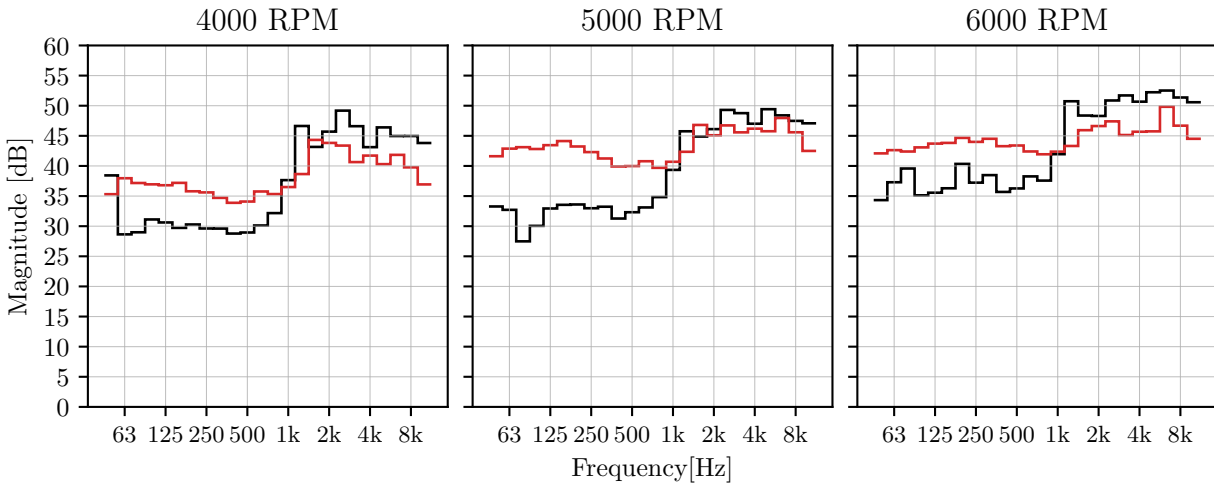

Fig. 10   One-third octave band levels of the broadband spectra at the three rotational speeds, considering the microphones on the propeller plane.

E. Directivities

Fig. 11 shows the directivities for the first, second, and third harmonics of the BPF, broadband noise, and OASPL. The directivity observed for the first harmonic exhibits a similar behavior, both in magnitude and shape, for the three rotational speeds. Higher variations are observed for the second and third harmonics' directivity. The results for broadband noise show similar directivities but differ in magnitude. No difference is observed between 5000 RPM and 6000 RPM directivities measured at the LVA-UFSC rig. This may explain the smaller differences observed for broadband directivity at 4000 RPM and 5000 RPM at the Delft rig. Finally, the overall SPL directivity is very similar between the two rigs, composed mostly of the first harmonic and broadband noise. At 4000 RPM, the Delft rig measures a slightly higher level due to the broadband component, whereas at 5000 RPM and 6000 RPM, the first harmonic dominance makes the overall levels very similar, even though the broadband directivity is more present on the overall directivity on the Delft facility than on the LVA-UFSC rig.

VI. Concluding Remarks

The objective of this paper was to compare measurements conducted with identical propellers on two different test rigs, analyzing thrust, torque, motor noise, and propeller noise, with a focus on the acoustic data. The main conclusions can be summarized as follows:

1) Results for broadband noise between test rigs consistently differed. The UFSC test rig displayed higher broadband noise at low frequencies, believed to be due to the propeller wake flowing around the rig structure. In that sense, a thinner and more aerodynamic structure may yield better results. Conversely, the Delft test rig displayed higher broadband noise at higher frequencies, possibly attributable to motor noise.

2) Motor noise can significantly impact propeller noise measurements at different frequency ranges (mid-frequency for the UFSC test rig and mid- to high-frequencies for the Delft test rig). Care should be taken when selecting the motor and defining its attachment to the structure. A subjective analysis of the UFSC results indicates that engine vibration may be transmitted to the structure, generating noise.

3) First harmonic and overall sound pressure levels for both test rigs were very similar, with a maximum difference of 2.8 dB overall.

4) Second and third harmonics are more sensitive to inflow conditions and installation effects, making it more difficult to achieve good agreement.
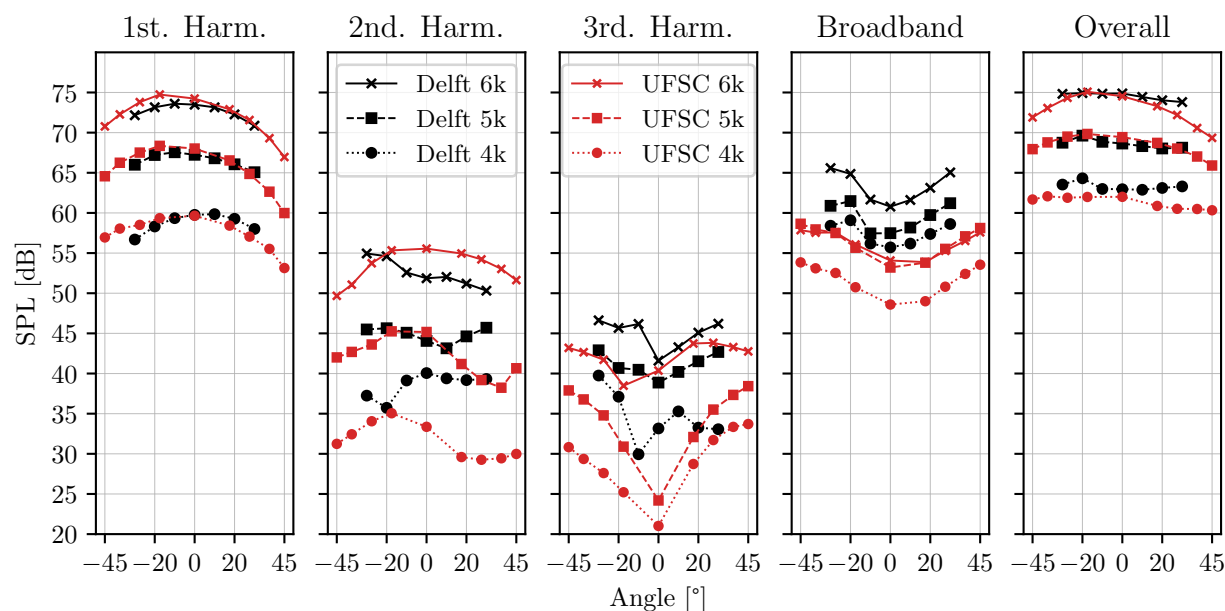
Fig. 11   Directivities for the first, second and third harmonics, for the broadband level and OASPL.

References

[1] Tom, L., Khowja, M., Vakil, G., and Gerada, C., "Commercial Aircraft Electrification—Current State and Future Scope," *Energies 2021, Vol. 14, Page 8381*, Vol. 14, No. 24, 2021, p. 8381. https://doi.org/10.3390/EN14248381, URL https://www.mdpi.com/1996-1073/14/24/8381/htm, publisher: Multidisciplinary Digital Publishing Institute.

[2] Rothfeld, R., Straubinger, A., Fu, M., Al Haddad, C., and Antoniou, C., "Chapter 13 - Urban air mobility," *Demand for Emerging Transportation Systems*, edited by C. Antoniou, D. Efthymiou, and E. Chaniotakis, Elsevier, 2020, pp. 267–284. https://doi.org/10.1016/B978-0-12-815018-4.00013-9, URL https://www.sciencedirect.com/science/article/pii/B9780128150184000139.

[3] Qi, F., Zhu, X., Mang, G., Kadoch, M., and Li, W., "UAV Network and IoT in the Sky for Future Smart Cities," *IEEE Network*, Vol. 33, No. 2, 2019, pp. 96–101. https://doi.org/10.1109/MNET.2019.1800250, publisher: Institute of Electrical and Electronics Engineers Inc.

[4] Barzkar, A., and Ghassemi, M., "Electric power systems in more and all electric aircraft: A review," *IEEE Access*, Vol. 8, 2020, pp. 169314–169332. https://doi.org/10.1109/ACCESS.2020.3024168, publisher: Institute of Electrical and Electronics Engineers Inc.

[5] Smith, M. J. T., *Aircraft noise*, Cambridge University Press, 1989. Pages: 382.

[6] Kurtz, D. W., and Marte, J. E., "A review of aerodynamic noise from propellers, rotors, and lift fans," Tech. Rep. NASA-CR-107568, Jan. 1970. URL https://ntrs.nasa.gov/citations/19700005920, nTRS Author Affiliations: Jet Propulsion Lab., California Inst. of Tech. NTRS Document ID: 19700005920 NTRS Research Center: Legacy CDMS (CDMS).

[7] Brentner, K. S., and Farassat, F., "Modeling aerodynamically generated sound of helicopter rotors," *Progress in Aerospace Sciences*, Vol. 39, No. 2-3, 2003, pp. 83–120. https://doi.org/10.1016/S0376-0421(02)00068-4, publisher: Pergamon.

[8] Casalino, D., Romani, G., Zhang, R., and Chen, H., "Lattice-Boltzmann calculations of rotor aeroacoustics in transitional boundary layer regime," *Aerospace Science and Technology*, Vol. 130, 2022, p. 107953. https://doi.org/10.1016/j.ast.2022.107953, URL https://www.sciencedirect.com/science/article/pii/S1270963822006277.

[9] Casalino, D., Romani, G., Pii, L. M., and Colombo, R., "Flow confinement effects on sUAS rotor noise," *Aerospace Science and Technology*, Vol. 143, 2023, p. 108756. https://doi.org/10.1016/j.ast.2023.108756, URL https://www.sciencedirect.com/science/article/pii/S1270963823006521.

[10] Zawodny, N., Boyd Jr, D., and Burley, C., "Acoustic characterization and prediction of representative, small-scale rotary-wing unmannedaircraft system components," *Proceedings of the 72nd Annual Forum of the American Helicopter Society*, West Palm Beach, FL, USA, 2016.

[11] Casalino, D., Grande, E., Romani, G., Ragni, D., and Avallone, F., "Definition of a benchmark for low Reynolds number propeller aeroacoustics," *Aerospace Science and Technology*, Vol. 113, 2021, p. 106707. https://doi.org/10.1016/j.ast.2021.106707, URL https://www.sciencedirect.com/science/article/pii/S1270963821002170.

[12] Tinney, C. E., and Sirohi, J., "Multirotor Drone Noise at Static Thrust," *AIAA Journal*, Vol. 56, No. 7, 2018, pp. 2816–2826. https://doi.org/10.2514/1.J056827, URL https://arc.aiaa.org/doi/10.2514/1.J056827, publisher: American Institute of Aeronautics and Astronautics.

[13] Wu, H., Jiang, H., Zhou, P., Zhong, S., Zhang, X., Zhou, G., and Chen, B., "On identifying the deterministic components of propeller noise," *Aerospace Science and Technology*, Vol. 130, 2022, p. 107948. https://doi.org/10.1016/J.AST.2022.107948, URL https://linkinghub.elsevier.com/retrieve/pii/S1270963822006228, publisher: Elsevier Masson.

[14] Stoica, L. G., Marco, A. D., and Camussi, R., "VENUS PROJECT: INVESTIGATION OF DISTRIBUTED PROPULSION NOISE AND ITS MITIGATION THROUGH WIND TUNNEL EXPERIMENTS AND NUMERICAL SIMULATIONS," *10th Convention of the European Acoustics Association*, Torino, Italy, 2023. URL https://appfa2023.silsystem.solutions/atti/001126.pdf.

[15] Beausse, Y., Cotté, B., Doaré, O., Pascal, C., Toralba, T., and Chapoutot, A., "EFFECT OF ROUGHNESS ON THE AEROACOUSTIC PERFORMANCE OF ROTOR NOISE AT LOW REYNOLDS NUMBER," *10th Convention of the European Acoustics Association*, Torino, Italy, 2023. URL https://appfa2023.silsystem.solutions/atti/000753.pdf.

[16] Acevedo Giraldo, D., Roger, M., and Jacob, M. C., "Experimental Study of the Aerodynamic Noise of a Pair of Pusher-Propellers Installed Over a Wing," *AIAA AVIATION 2023 Forum*, AIAA AVIATION Forum, American Institute of Aeronautics and Astronautics, 2023. https://doi.org/10.2514/6.2023-3359, URL https://arc.aiaa.org/doi/10.2514/6.2023-3359.

[17] Bonomo, L. A., Cordioli, J. A., Colaciti, A. K., Fonseca, J. V. N., and Sim?es, L. G., "Assessment of the Performance of Tonal-Broadband Decomposition Algorithms for Propeller Noise," *AIAA AVIATION 2023 Forum*, AIAA AVIATION Forum, American Institute of Aeronautics and Astronautics, 2023. https://doi.org/10.2514/6.2023-3218, URL https://arc.aiaa.org/doi/10.2514/6.2023-3218.

[18] Willshire Jr, W., and Nystrom, P., "Investigation of effects of microphone position and orientation on near-ground noise measurements," NASA Technical Report L-15097 NAS 1.60:2004 NASA-TP-2004, Langley, VA, USA, 2004. URL https://ntrs.nasa.gov/citations/19840002845.

[19] Weitsman, D., Stephenson, J. H., and Zawodny, N. S., "Effects of flow recirculation on acoustic and dynamic measurements of rotary-wing systems operating in closed anechoic chambers," *The Journal of the Acoustical Society of America*, Vol. 148, No. 3, 2020, p. 1336. https://doi.org/10.1121/10.0001901, URL https://asa.scitation.org/doi/abs/10.1121/10.0001901, publisher: Acoustical Society of America ASA.

[20] Grande, E., Ragni, D., Avallone, F., and Casalino, D., "Laminar Separation Bubble Noise on a Propeller Operating at Low Reynolds Numbers," *American Institute of Aeronautics and Astronautics (AIAA)*, Vol. 60, 2022, pp. 5324–5335. https://doi.org/10.2514/1.j061691, URL https://pure.tudelft.nl/ws/portalfiles/portal/131821948/1.J061691.pdf.

[21] Sree, D., and Stephens, D. B., "Improved Separation of Tone and Broadband Noise Components from Open Rotor Acoustic Data," *Aerospace 2016, Vol. 3, Page 29*, Vol. 3, No. 3, 2016, p. 29. https://doi.org/10.3390/AEROSPACE3030029, URL https://www.mdpi.com/2226-4310/3/3/29/htm, publisher: Multidisciplinary Digital Publishing Institute.